Island Arc (2008) **17,** 70–89

Research Article

Evolution of West Rota Volcano, an extinct submarine volcano in the southern Mariana Arc: Evidence from sea floor morphology, remotely operated vehicle observations and ^{40}Ar–^{39}Ar geochronological studies

ROBERT J. STERN,[1,*] YOSHIHIKO TAMURA,[2] ROBERT W. EMBLEY,[3] OSAMU ISHIZUKA,[4] SUSAN G. MERLE,[3] NEIL K. BASU,[1] HIROSHI KAWABATA[2] AND SHERMAN H. BLOOMER[5]

[1]*Geosciences Department, University of Texas at Dallas, Richardson TX 75083-0688, USA (email: rjstern@utdallas.edu),* [2]*Institute for Research on Earth Evolution (IFREE), Japan Agency for Marine-Earth Science and Technology (JAMSTEC), Yokosuka 237-0061, Japan,* [3]*Pacific Marine Environmental Laboratory NOAA, 2115 SE O.S.U. Dr., Newport, OR 97365-5258, USA,* [4]*Institute of Geosciences, Geological Survey of Japan/ AIST, Tsukuba 305-8567, Japan, and* [5]*College of Science, Oregon State University, 128 Kidder Hall, Corvallis, OR 97331-4608, USA*

Abstract West Rota Volcano (WRV) is a recently discovered extinct submarine volcano in the southern Mariana Arc. It is large (25 km diameter base), shallow (up to 300 m below sealevel), and contains a large caldera (6×10 km, with up to 1 km relief). The WRV lies near the northern termination of a major NNE-trending normal fault. This and a second, parallel fault just west of the volcano separate uplifted, thick frontal arc crust to the east from subsiding, thin back-arc basin crust to the west. The WRV is distinct from other Mariana Arc volcanoes: (i) it consists of a lower, predominantly andesite section overlain by a bimodal rhyolite-basalt layered sequence; (ii) andesitic rocks are locally intensely altered and mineralized; (iii) it has a large caldera; and (iv) WRV is built on a major fault. Submarine felsic calderas are common in the Izu and Kermadec Arcs but are otherwise unknown from the Marianas and other primitive, intraoceanic arcs. ^{40}Ar–^{39}Ar dating indicates that andesitic volcanism comprising the lower volcanic section occurred 0.33–0.55 my ago, whereas eruption of the upper rhyolites and basalts occurred 37–51 thousand years ago. Four sequences of rhyolite pyroclastics each are 20–75 m thick, unwelded and show reverse grading, indicating submarine eruption. The youngest unit consists of 1–2 m diameter spheroids of rhyolite pumice, interpreted as magmatic balloons, formed by relatively quiet effusion and inflation of rhyolite into the overlying seawater. Geochemical studies indicate that felsic magmas were generated by anatexis of amphibolite-facies meta-andesites, perhaps in the middle arc crust. The presence of a large felsic volcano and caldera in the southern Marianas might indicate interaction of large normal faults with a mid-crustal magma body at depth, providing a way for viscous felsic melts to reach the surface.

Key words: bimodal magmatism, hydrothermal mineralization, Mariana Arc, pumice, Quaternary volcano, submarine caldera.

INTRODUCTION

The 3000-km long Izu–Bonin–Mariana (IBM) Arc system is an outstanding example of a juvenile, intraoceanic convergent plate margin, which has become the particular focus of US and Japanese efforts to understand the operation of the 'Subduction Factory' (Tatsumi & Stern 2006). West Rota Volcano (WRV) is an extinct (or long dormant) submarine volcano in the southern part of the Mariana Arc, located approximately 40 km WNW of Rota Island, Commonwealth of the Northern Mariana Islands (Fig. 1). It and Esmeralda Bank to the

*Correspondence.

Received 8 September 2006; accepted for publication 12 August 2007.

doi:10.1111/j.1440-1738.2007.00600.x

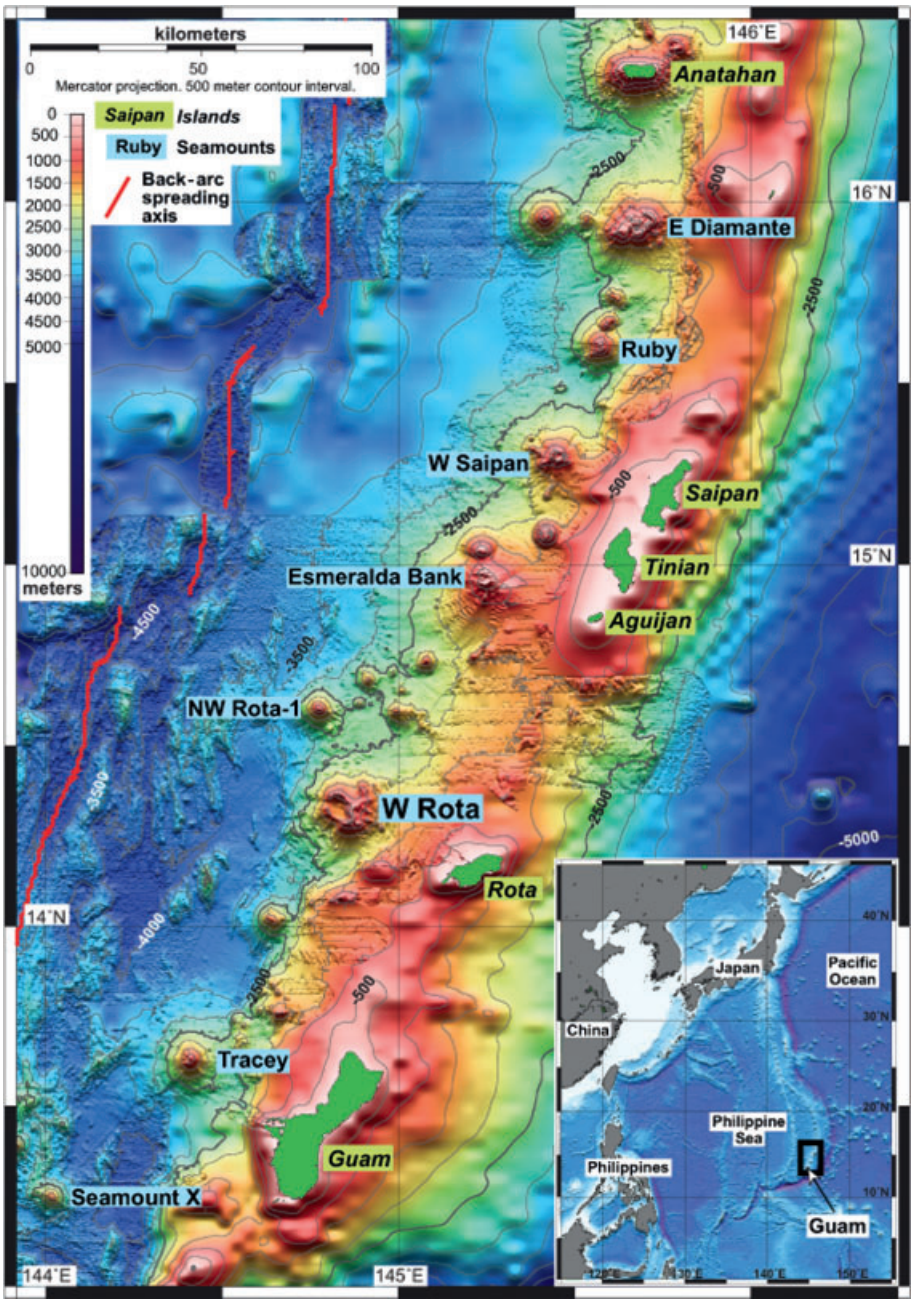

Fig. 1 Locality map for the Southern Seamount Province (SSP) of the Mariana Arc (Mercator projection, 500 m contour interval). Anatahan is the southernmost volcano of the Central Island Province, SSP extends from Diamante cross-chain south at least to Seamount X. Data sources: NOAA Vents EM300 and SeaBeam 2000 multibeam bathymetry, Cook 6 & 7 HMR1 bathymetry, and bathymetry based on inversion of satellite altimetry (Smith & Sandwell 1997). Back-arc spreading center axis positions provided by Fernando Martinez. Bathymetry data are 200 m grid cell size. Satellite data subsampled to 200 m from 3500 m cell size. Island names are italicized. Inset shows location of figure in Western Pacific.

north (Fig. 1) are the largest volcanoes in the Mariana Southern Seamount Province (Bloomer *et al.* 1989).

Compared to other Mariana Arc volcanoes, WRV is remarkable for several reasons: (i) it consists of a lower section of predominantly andesite overlain by a layered bimodal rhyolite-basalt sequence; (ii) andesitic rocks are locally intensely altered and mineralized; (iii) it has a large caldera; and (iv) it is built on a major fault. Large calderas are commonly associated with volcanoes that erupt voluminous felsic lava, typically >60 wt% SiO_2 (WRV rhyolite pumice contains *ca* 72 wt% SiO_2). Such volcanoes are common both along the Izu (Fiske *et al.* 2001) and Kermadec (Wright *et al.* 2006) arcs but are otherwise unknown from the Mariana Arc and are not reported from other intraoceanic arcs. The WRV's caldera is large compared with Izu and Kermadec felsic calderas – although Macauley Caldera in the Kermadecs is the same size (Wright *et al.* 2006). The WRV caldera dimensions are similar to those of more famous calderas, such as Krakatoa in Indonesia and Crater Lake in the Cascades (Fig. 2).

Calderas are natural targets of volcanological study because the steep caldera walls often expose

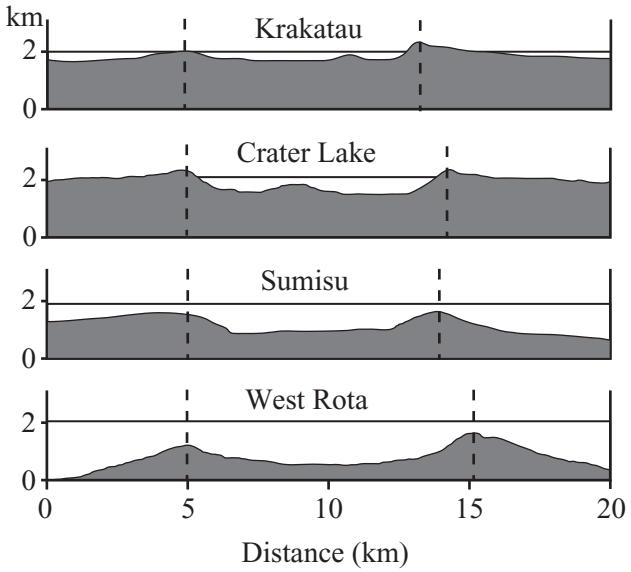

Fig. 2 Comparison of the size of West Rota Caldera with that of other felsic calderas using profiles to approximate caldera diameter: Krakatau (Indonesia), Crater Lake (Oregon, USA), Sumisu (Izu, Japan) and West Rota. The vertical lines indicate the caldera rims. No vertical exaggeration. Krakatau and Crater Lake profiles are modified from Fiske *et al.* (2001).

a significant part of the volcanic stratigraphy. Even though submarine calderas require ships and thus are relatively expensive to study, they have some advantages over subaerial calderas, the walls of which are quickly degraded by erosion and have steep and unstable slopes that are often dangerous to climb. In contrast, submarine caldera walls are easily studied using a remotely operated vehicle (ROV), which is connected to the research vessel and can rise through the water column, inspecting and sampling layers as it ascends.

Here we present multibeam swathmapping and backscatter imagery of WRV and ROV sea floor examination of it, emphasizing its history. The current report summarizes our present understanding of WRV and is intended to be a progress report, as well as provide a sound basis for future research. To provide temporal context for the volcano's evolution, we also report the results of Ar–Ar dating on igneous rock samples. This work also provides context for ongoing petrological studies.

MARINE GEOLOGICAL AND GEOPHYSICAL INVESTIGATIONS

Table 1 summarizes dredge and ROV investigations of WRV. The WRV was first identified and sampled in 1979 during the Scripps Institution of

Table 1 Dredge and remotely operated vehicle (ROV) studies of West Rota Volcano

	Dredge 47	Dredge 63	Dredge 64	Dredge 65	Dredge 66	R-785	HD-482	HD-483	HD-484	HD-489
Cruise	MARIANA	COOK 7†	COOK 7	COOK 7	COOK 7	TT167‡	NT05-17	NT05-17	NT05-17	NT05-17
Ship	*Washington*	*Melville*	*Melville*	*Melville*	*Melville*	*Thompson*	*Natsushima*	*Natsushima*	*Natsushima*	*Natsushima*
ROV	–	–	–	–	–	ROPOS	Hyper-Dolphin	Hyper-Dolphin	Hyper-Dolphin	Hyper-Dolphin
Year	1979	2001	2001	2001	2001	2004	2005	2005	2005	2005
Start										
Lat. (N)	14°19.8′	14°20′	14°17.35′	14°16.2′	14°18.95′	14°20.034′	14°19.661′	14°17.739′	14°20.079′	14°16.214′
Long. (E)	144°54.1′	144°50.93′	144°54.3′	144°56.69′	144°50.95′	144°50.97′	144°51.098′	144°51.13′	144°50.666′	144°53.741′
Depth (m)	889	1326	1145	1732	1308	1248	1012	1150	1391	1229
Finish										
Lat. (N)	14°19.6′	14°20′	14°17.55′	14°16.25′	14°19.01′	14°19.776′	14°19.433′	14°17.644′	14°20.747′	14°16.887′
Long. (E)	144°52.4′	144°51.23′	144°54.53′	144°56.69′	144°51.1′	144°51.87′	144°51.669′	144°51.694′	144°51.400′	144°52.035′
Depth (m)	505	1070	900	1524	327	462	414	662	642	491
Reference	Dixon and Stern (1983)									

†HMR-1 swarthmapping during Leg 7 of the 2001 COOK expedition, http://www.soest.hawaii.edu/HMRG/MR1/index.html; ‡NOAA 2004 TT167 cruise, http://oceanexplorer.noaa.gov/explorations/04fire/welcome.html; ROV, remotely operated vehicle, http://en.wikipedia.org/wiki/ROV. ROPOS, http://www.ropos.com/ Hyper-Dolphin, http://www.jamstec.go.jp/jamstec-e/rov/

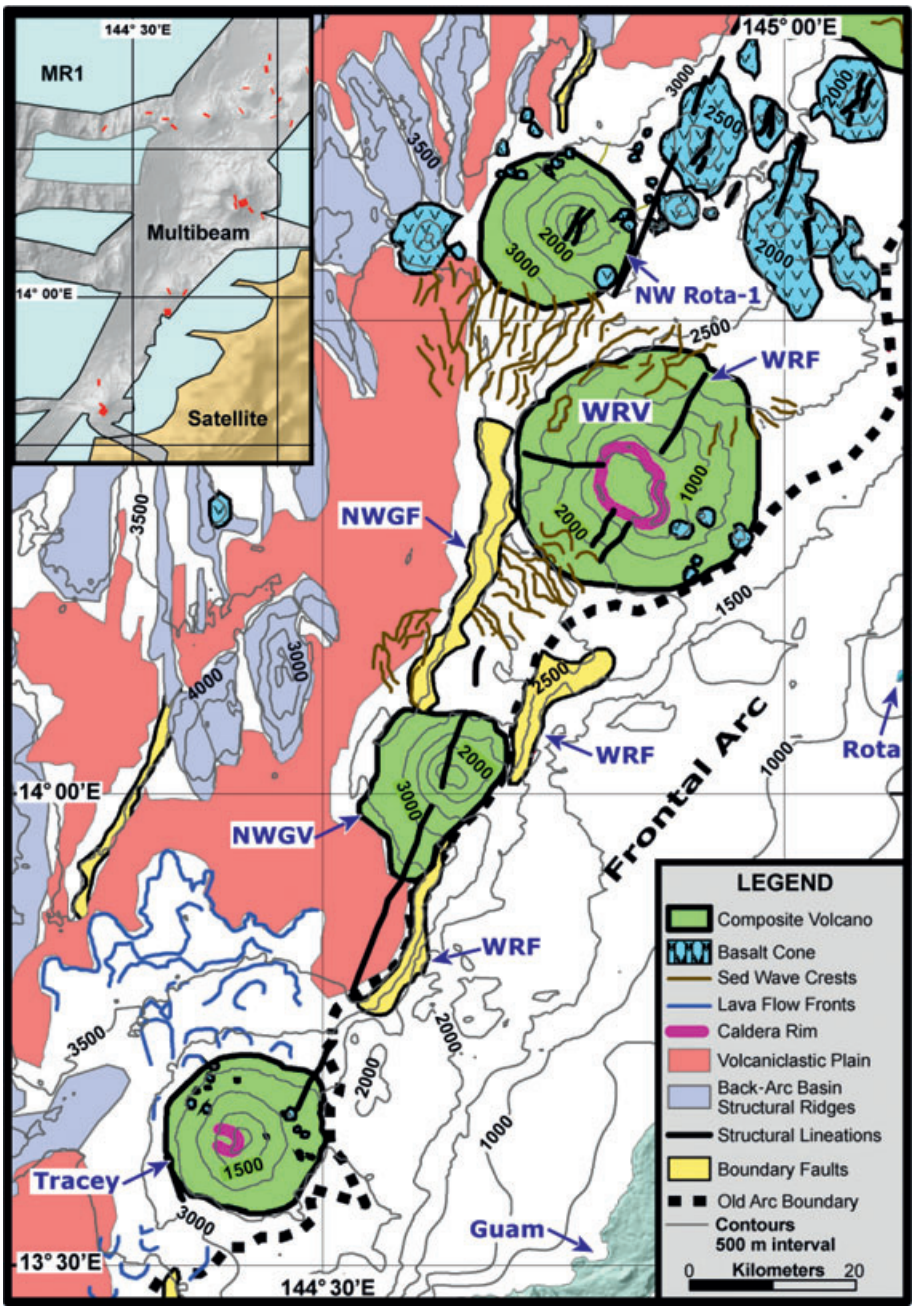

Fig. 3 Morphological features of the southern Mariana Arc. Interpretation based on bathymetry, sidescan sonar, and sea floor sampling; mapping coverage is shown in inset. Multibeam data includes 30 kHz EM300 system on R/V *T. G. Thompson*, 50 kHz SeaBat system on *R.V. Natsushima* & SeaBeam 2000 on *R/V Melville*. Most of the area was also surveyed by HMR1 sea floor imaging system (Rognstad 1992), which output both acoustic backscatter (in sidescan mode) and phased array bathymetry. The lower precision HMR1 bathymetry was only used in the absence of the multibeam coverage. These data were overlayed in the ESRI Arcmap program for interpretation. WRF, West Rota Fault; NWGF, Northwest Guam Fault; WRV, West Rota Volcano; NWGV, Northwest Guam Volcano; EsmV, Esmeralda Volcano.

Oceanography MARIANA expedition. One dredge (D47, Fig. 3) near the summit recovered andesite and abundant rhyolite pumice (Dixon & Stern 1983), but the caldera was not known until Hawaii MR-1 swathmapping during Leg 7 of the 2001 Cook expedition.

Sea floor bathymetry and sonar backscatter data was obtained during 2001 Cook 7, several NOAA cruises and JAMSTEC NT05-17. Hawaii MR1 is a shallow-towed sidescan sonar system that also provides relatively low resolution bathymetry (Edwards 2007). Bathymetry collected by NOAA expeditions used a Simrad EM300 multibeam sonar system mounted on the hull of the R/V *Thomas G. Thompson*. Different regions mapped by these expeditions are shown in Appendix Figure A1.

Four dredge samplings of WRV occurred during Cook 7 (D63-66, Fig. 3). D63 from the eastern caldera wall recovered 250 kg of diverse lithologies, including hydrothermally altered rocks, abundant dacite pumice and large blocks of fresh basalt. D64 and D65 sampled two parasitic cones on the volcano's southeast flank and recovered abundant basalt and pumice from both. D66 from

the caldera wall just south of D63 recovered only abundant pumice.

The first ROV dive was carried out using ROPOS (Shepherd 2007) during TT167 in April 2004 (R-785), followed by four dives with Hyper-Dolphin (Kato 2007) aboard the R/V *Natsushima* during NT05-17 in October 2005 (HD-482, 483, 484 and 489). Four of the five ROV dives examined stratigraphy exposed in the eastern caldera wall, and the last dive (HD-489) traversed two parasitic cones on the volcano's southeast flank.

TECTONIC SETTING OF THE SOUTHERN MARIANA ARC

Regional swath-mapping shows that WRV lies on a major NNE-trending normal fault, named here the West Rota Fault (WRF; Fig. 3). A few km southwest of WRV, the WRF has approximately 1200 m of apparent vertical offset, diminishing to a few hundred meters at WRV itself, suggesting that the most important WRF offsets pre-date caldera formation. This interpretation is tempered because the fault cannot be identified northeast of WRV. The WRF is greatly subdued where it transects WRV, but its location might be manifested by bathymetric re-entrants (Fig. 4) and perhaps a fault observed on the caldera floor during dive HD-484, although this fault trends NNW.

Another, more northerly trending normal fault lies *ca* 20 km west of the WRF and has *ca* 1 km of relief; this is called the Northwest Guam Fault (NWGF; Fig. 3). The WRF and NWGF reactivate a fundamental crustal boundary: uplifted, thick crust and lithosphere beneath the frontal arc to the east and subsiding, thin back-arc basin crust and lithosphere to the west. The two faults are interpreted to be associated with recent uplift of

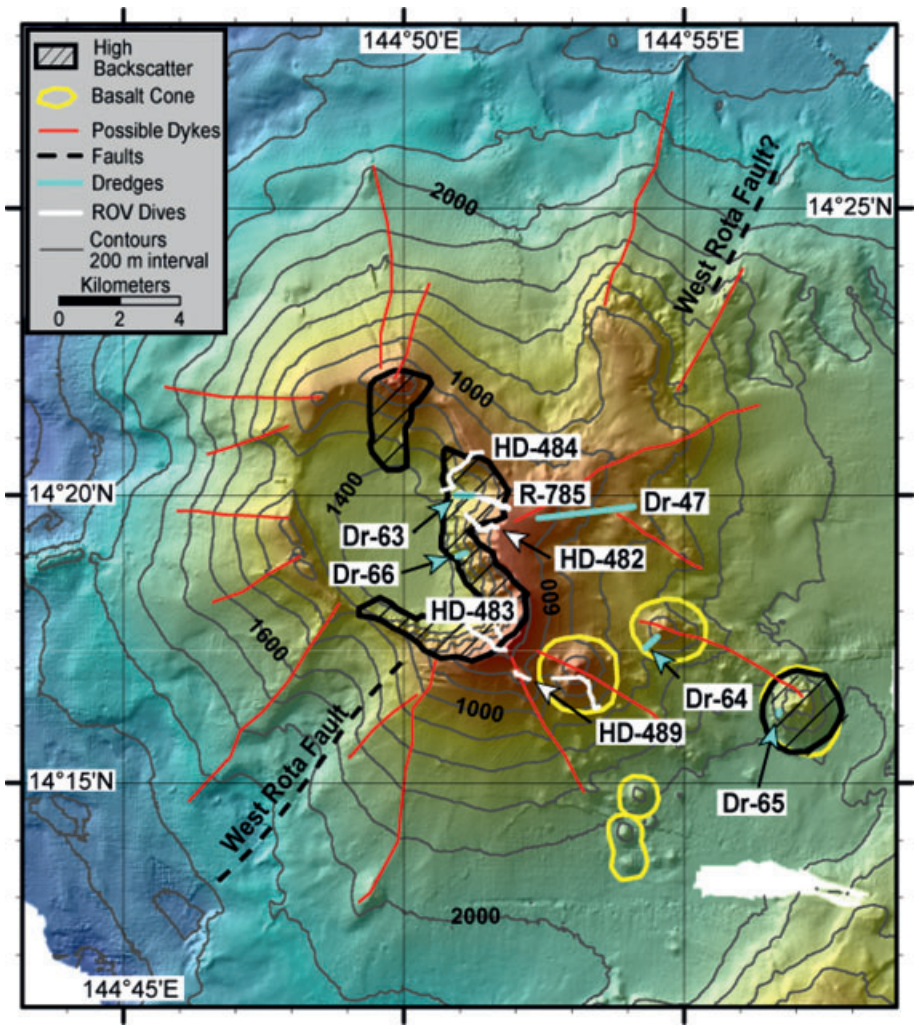

Fig. 4 Bathymetry and surface interpretation of West Rota Volcano, based on 25 m grid of EM300 multibeam sonar, sidelit from northwest. Diagonal stripes mark areas of high sonar backscatter probably indicating steep crop outs; other surfaces show low sonar backscatter and are probably covered with pumice. Orange lines approximate inferred radial dykes. Dashed black line labeled 'WRF' is the inferred West Rota Fault Zone. Dark shaded areas are high backscatter lava cones. White lines mark remotely operated vehicle (ROV) bottom tracks.

the southern Mariana frontal arc. This neotectonism is also associated with rapid sea floor spreading in the southern Mariana Trough (Martinez *et al.* 2000; Kato *et al.* 2003) and rapid trench rollback along the Challenger Deep segment of the Mariana Trench (Fryer *et al.* 2003; Gvirtzman & Stern 2004). A three-component magnetometer survey during Cook 7 identified back-arc basin crust along the eastern margin of the Mariana Trough that was magnetized during the Gauss normal-polarity chron (2.60–3.58 Ma; Ishihara *et al.* 2001). This provides an upper age limit for the WRF and WRV, which was built on or near this crust.

Although it has long been inferred that Mariana Arc volcanoes are situated on or near the easternmost bounding faults of the back-arc basin (Bloomer *et al.* 1989), WRV is the only Mariana Arc volcano where this can be demonstrated. It is likely that the abundance of felsic eruptive products and large formation of the caldera, unique for the Mariana Arc, is related to the WRF, as discussed below.

The WRV lies just south of another important tectonic boundary, the 14°40′N slab discontinuity (Miller *et al.* 2006). The discontinuity controls the location of an unusual volcanic cross-chain (Figs 1, 4), which includes the active northwest Rota-1 volcano (Embley *et al.* 2006) and Chaife Seamount, which erupts unusually magnesian lavas (Kohut *et al.* 2006).

MORPHOTECTONICS OF WEST ROTA VOLCANO

The most striking feature of WRV is its large caldera (Fig. 4). This is elliptical in map view, 6–10 km across with the long axis oriented NNW–SSE. The featureless caldera floor lies at a maximum depth of 1500 m below sealevel (BSL). Simple extrapolation of the volcanic slopes upward suggests that WRV might have once been an island, with a summit that could have stood several hundreds of meters above sealevel.

Fly-through movies showing sonar backscatter draped on bathymetry for the entire Mariana Arc and for WRV can be downloaded from the NOAA Ocean Exploration website: (Merle & Carothers 2007).

The WRF exerts important controls on WRV. The caldera is built above the WRF near its apparent northeast termination. WRF trends NNE up the southwest slope, where bathymetric contours are deflected *ca* 2 km towards the caldera, but it cannot be confidently traced northeast of the volcano. The fact that the southeast rim reaches within 304 m of the sea surface, whereas the shallowest part of the western rim is *ca* 1000 m BSL suggests that the WRF uplifted the eastern WRV relative to the western WRV. The fault trend divides WRV outer slopes into an eastern half with complex relief and a much smoother western half (Fig. 4); these lie on either side of the WRF. This difference in morphology does not reflect the different sonar systems used to map the volcano, because the morphotectonic subdivisions do not correspond to regions mapped by different systems (compare Fig. 4 and Appendix Fig. A1). The ruggedness of the eastern WRV is principally caused by numerous parasitic cones along the southeast neovolcanic zone and by a structural bulwark as shallow as 800 m BSL in the northeast. The northeast high might manifest parts of the volcano that were relatively uplifted along the WRF, or it might represent the preserved flank of an older caldera. There is also extensive medium-scale (*ca* 200 m wavelength) roughness on the volcano flank east of 144°52′E that is not seen in the west (Fig. 4); we have no idea what caused this.

Interpretation of sonar backscatter images (Fig. 4) indicates that the eastern caldera wall has more outcrops of precaldera rocks, whereas the western caldera wall appears 'backscatter-smooth', suggesting thick pumice cover. These observations might indicate that the climactic eruption was largely directed towards the lower, western sector of the volcano.

Caldera bathymetry suggests formation by piston-like, coherent subsidence (Lipman 1997). The subdued caldera floor relief suggests it might be underlain by a thick section of intracaldera tuff and slide breccia (see fig. 3 of Lipman 1997). The ROV observations during TT167 dive R-785 indicate that most of the caldera floor is composed of loose pumice, consistent with this interpretation.

PETROLOGICAL SYNOPSIS

The magmatic evolution of WRV is currently the focus of ongoing study; however, a summary of the composition of its lavas is instructive for understanding the evolution of the volcano.

Low-K suites characterize the Izu segment of the IBM Arc system, whereas medium-K suites typify the Mariana segment, with a high-K 'shoshonitic' suite characterizing the Izu–Bonin to

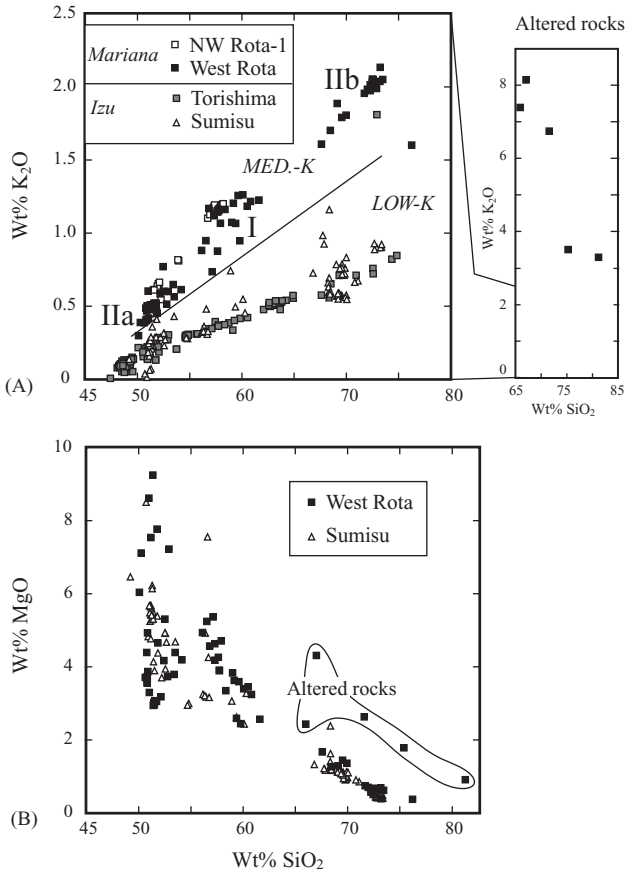

Fig. 5 (a) K_2O versus SiO_2 (wt%) for lavas from Sumisu and Torishima Volcanoes (Izu Arc) and West Rota and NW Rota-1 Volcanoes (Mariana Arc). Medium-, and low-K boundaries after Gill (1981). Data for fresh lavas from Tamura *et al.* (unpubl. data, 2007) and Basu (2006). Panel on right show compositions of hydrothermally altered andesitic (lower section) lavas, data from Basu (2006). Low-K suites characterize the Izu Arc and a medium-K typifies the Mariana Arc. Numeral I corresponds to andesites of the lower volcanic succession, whereas IIa-IIb correspond to bimodal suite of the upper stratigraphic section, as discussed in text. (b) MgO versus SiO_2 (wt%) for lavas from West Rota and Sumisu Volcanoes. Volcanic rocks from both of the caldera volcanoes span a similar compositional range, from basalt to rhyolite. Note also the presence of a silica gap of >6 wt% SiO_2, separating andesite compositions from those of dacites and rhyolites.

Mariana transition (Stern *et al.* 2003). This systematic difference is shown in Figure 5a, which shows K_2O versus SiO_2 in volcanic rocks from West Rota and NW Rota-1 (Embley *et al.* 2006) in the Mariana Arc, and Sumisu and Torishima in the Izu Arc. The lavas from WRV define a medium-K suite that is typical of Mariana Arc lavas. Figure 5b shows MgO versus SiO_2 in lavas from West Rota and Sumisu. Both caldera volcanoes have similar MgO contents for a given SiO_2 and interestingly, both volcanoes have a SiO_2 gap between andesite (*ca* 60 wt% SiO_2) and dacite (>65 wt% SiO_2). This suggests that models which explain rhyolite genesis in Sumisu might be applicable for West Rota, and vice versa, encouraging further development of a general model for the generation of IBM felsic magmas.

The WRV lavas and tuffs comprise two sequences: a lower sequence of dominantly andesitic lavas and breccia (I in Fig. 5a), and an upper bimodal sequence comprising basalts and basaltic andesites (IIa in Fig. 5a), along with dacites and rhyolites (IIb in Fig. 5a). The two sequences show transitional relationships; andesitic lavas were found high in the sequence (as shallow as 600 m during dive HD-482) and thin felsic tuffs were found low in the section (as deep as 940 m during dive HD-484). Mafic and felsic effusives in the upper sequence are intimately related, both spatially and stratigraphically. Felsic samples are mostly pumiceous, pervasively hydrated, friable and weakly consolidated and thus are difficult to representatively sample and analyze. Locally, the lower andesitic sequence has been intensely altered by hydrothermal fluids, including development of stockwork sulphide mineralization and intense potassic metasomatism (Fig. 5a, right). Most basalts are fractionated but some are quite primitive, with 7–9 wt% MgO. The thick pyroclastic sequences of rhyolite, with 72–74 wt% SiO_2 (Fig. 5), of West Rota are very unusual for the Mariana Arc. Mafic and felsic magmatism was intimately related, as is typical for other felsic volcanoes, such as Sumisu in the Izu Arc (Shukuno *et al.* 2006).

Ar–Ar GEOCHRONOLOGY

Six fresh volcanic samples were selected for ^{40}Ar–^{39}Ar age determinations. Four samples of upper sequence basalt and dacite were analyzed at the Geological Survey of Japan/AIST (Uto *et al.* 1997), and two samples of fresh andesite from the lower part of the volcanic sequence were analyzed at Oregon State University. Analytical procedures at GSJ/AIST are reported in Ishizuka *et al.* (2003). Samples were treated ultrasonically in 3 N HCl and then 4 N HNO_3 for 10–15 min to remove possible secondary phases (e.g. carbonates, hydrated glass) before irradiation of 13–14 mg groundmass aliquots. Sanidine from the Fish Canyon Tuff (FC3) was used as flux monitor and assigned an age of 27.5 Ma (Uto *et al.* 1997; Lanphere & Baadsgaard 2001). Correction for interfering isotopes was achieved by analyses of $CaFeSi_2O_6$ and $KFeSiO_4$ glasses irradiated with the samples. Step-heating was accomplished with a laser. The

Table 2 ^{40}Ar–^{39}Ar geochronology results

Sample no.	Lithology	Latitude (N)	Longitude (E)	Depth (m)	Plateau age (Ka)	Isochron age (Ka)	Initial $^{40}Ar/^{36}Ar$	Lab
R-785–5	Andesite	14°20.01′	144°51.15′	1144	347 ± 14	344 ± 65	297 ± 48	OSU
R-785–9	Andesite	14°19.88′	144°51.64′	779	527 ± 117	496 ± 255	296 ± 4	OSU
HD-483R20	Hb-pyx rhyolite dyke	14°17.67′	144°51.68′	678	37 ± 6	34 ± 7	300 ± 5	AIST
HD-489R5	Hb rhyolite dyke	14°16.25′	144°53.64′	1148	51 ± 30	59 ± 15*	297 ± 2	AIST
HD-489-R19	Hb rhyolite	14°16.79′	144°52.47′	819	470 ± 60	450 ± 130	296 ± 4	AIST
HD-489-R20	Pl-phyric basalt	14°16.81′	144°52.41′	768	110 ± 100	–	305 ± 4	AIST

^{40}Ar–^{39}Ar age spectra and inverse isochron plots are shown in Figure 6. *isochron data using all steps, which is regarded as the best estimate for this analysis. AIST, Japan National Institute of Advanced Industrial Science and Technology; OSU, Oregon State University.

GSJ/AIST system blank was 7.5×10^{-14} mL standard temperature and pressure (STP) for ^{36}Ar, 2.5×10^{-13} mL STP for ^{37}Ar, 2.5×10^{-13} mL STP for ^{38}Ar, 1.0×10^{-12} mL STP for ^{39}Ar and 2.5×10^{-12} mL STP for ^{40}Ar. A blank analysis was done every time after two or three analyses. All errors for ^{40}Ar–^{39}Ar results are reported at one standard deviation and include analytical uncertainties for isotopic analysis, correction for interfering isotopes and *J*-value estimation. An error of 0.5% was assigned to *J*-values as a pooled estimate for the present study. Age plateaus were determined following the definition by Fleck *et al*. (1977). Inverse isochrons were calculated using York's least-squares fit, which accommodates errors in both ratios and correlations of errors (Fleck *et al*. 1977). Results are summarized in Table 2 and plotted in Figure 6.

The andesite sample that gave the best age (R785-5; plateau age = 347 ± 14 Ka, isochron age = 344 ± 65 Ka) was recovered as float on the caldera floor near the caldera wall. Another sample, a clast in an andesitic volcaniclastic flow taken from exposures near the base of the caldera wall (R785-9; plateau and isochron ages of 527 ± 117 and 496 ± 255 Ka) gave a poorer and older age. Both samples gave $(^{40}Ar/^{36}Ar)_0$ ~ atmospheric, so excess Ar is not a concern. We conclude that andesitic volcanism of the lower sequence was active *ca* 350 000 years ago and perhaps several hundred thousand years earlier. These ages also constrain caldera formation to younger than 350 000 years ago.

Three felsic dyke samples were dated: HD-483R20 (hornblende–pyroxene rhyolite dyke from southeast caldera wall), HD-489R5 (hornblende rhyolite dyke from southeast slope of WRV) and HD-483R2 (rhyolite dyke from inner caldera wall). HD-483R2 gave a very disturbed Ar release spectrum, which is not used or discussed further. HD-489R5 did not form a plateau in a strict sense, but the last four steps gave consistent ages, comprising 46% of released gas (Fig. 6a). The age from these steps is 51 000 ± 3000 years, whereas the isochron age calculated from all steps is 59 000 ± 15 000 years old. The best result came from HD-483R20, which gave a plateau age of 37 000 ± 6000 years; this is indistinguishable from an isochron age of 34 000 ± 7000 years (Fig. 6b). These samples also gave $(^{40}Ar/^{36}Ar)_0$ ~ atmospheric, so excess Ar is probably not a problem for these young lavas. Because felsic dykes are compositionally related to upper sequence pumiceous deposits, we conclude that felsic igneous activity on West Rota occurred 37–51 Ka ago; because the HD-483R20 dyke exposed in the inner trench wall must have been emplaced and cooled before being exposed as a result of caldera collapse; caldera collapse could not have occurred before its emplacement. We tentatively conclude that caldera formation occurred no earlier than 37–51 Ka.

HD-489 traversed parasitic cones on the southeast WRV, and two samples were dated. Seven consecutive steps in the mid-temperature range for hornblende rhyolite HD-489R19 released 56% of the gas, forming a plateau with an age of 0.47 ± 0.06 Ma. This is consistent with the inverse isochron age of 0.45 ± 0.13 Ma having $(^{40}Ar/^{36}Ar)_0$ intercept of 296 ± 4. Thus, 0.47 Ma approximates when this dacite erupted. Basalt sample HD-489R20 contains very little radiogenic ^{40}Ar and gave a disturbed age spectrum indicating that it is younger than *ca* 0.21 Ma. The older ages obtained for HD-489 samples compared to *ca* 37–51 Ka best estimate for the age of the caldera-forming event suggests that parasitic cones on the south WRV were active well before caldera collapse.

STRATIGRAPHY OF WEST ROTA VOLCANO

Four ROV dives looked at near-vertical sections along a 6 km sector of the eastern caldera wall; two

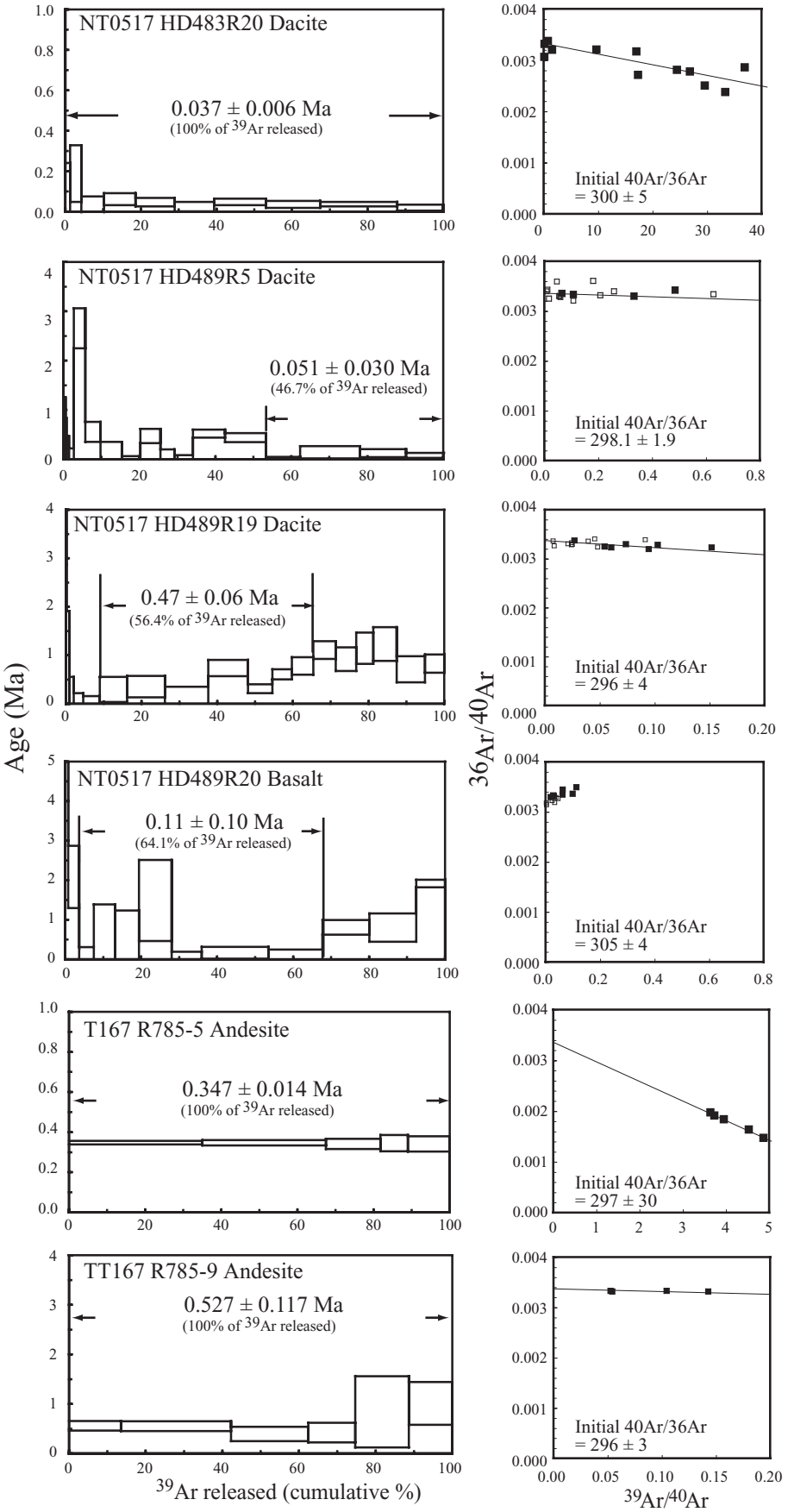

Fig. 6 ^{40}Ar–^{39}Ar age spectra (left) and inverse isochron plots (right) for groundmass samples of lavas from West Rota Volcano. Solid symbols in the inverse isochron plots are plateau forming steps. (a) HD483-R20. Southeast caldera wall at a depth of 678 m. Hb rhyolite dyke with 73.4 wt% SiO_2. (b) HD-489R5. Southeast flank of volcano near basaltic parasite cone at a depth of 1148 m. Hb rhyolite dyke with 72 wt% SiO_2. (c) HD489R19. Hb dacite with 71.7% SiO_2. Parasitic cone on southeast slope of West Rota at 810 m depth. (d) HD489R20. Parasitic cone on southeast slope of West Rota at 769 m depth. Pl-phyric basalt with 51.5% SiO_2 (e) R785-5. Float from east caldera floor at a depth of 1144 m. Pl-CPX andesite with 58% SiO_2. (f) R785-9. Base of east caldera wall at a depth of 779 m. Pl-CPX andesite with 60.9% SiO_2

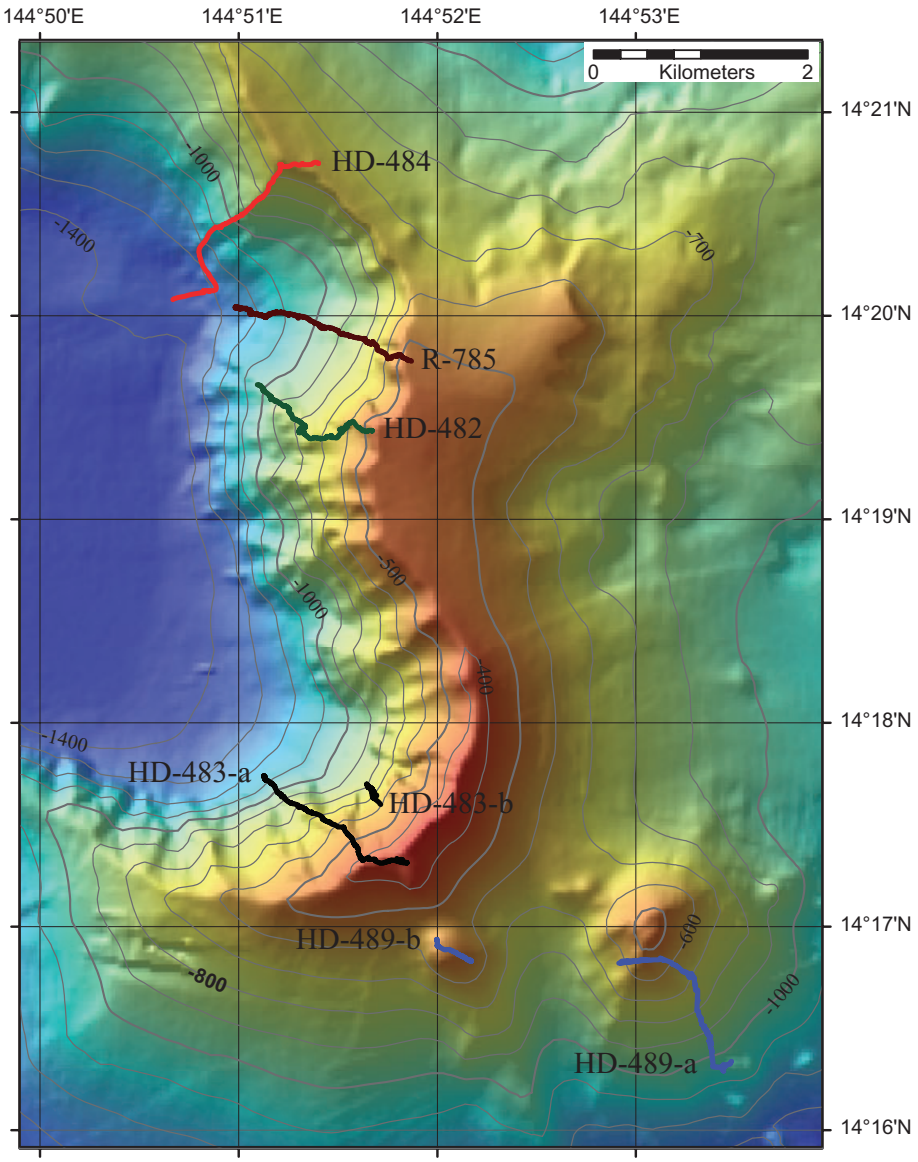

Fig. 7 Location of four remotely operated vehicle (ROV) transects on eastern caldera wall and 1 ROV transect on southeast flank of volcano. One dive (R785) was conducted using R/V *Melville* and ROPOS in 2004 and four dives (HD-482–484; HD-489) were carried out using R/V *Natsushima* and Hyper-Dolphin in 2005.

parasitic cones on the southeast upper flank were examined during one dive (Fig. 7). Each caldera wall dive encountered different stratigraphic sections; we conclude that WRV stratigraphy is complex and the picture we have of the volcanic succession is incomplete. The ROV observations were controlled with navigation and bathymetry, allowing stratigraphic sections for each of the transects to be constructed. These sections are summarized in Figure 8, and representative photographs are shown in Figures 9 and 10. Detailed stratigraphy of the pyroclastic section is shown in Figure 11.

Up to 900 m of volcanic stratigraphy is exposed in the steep eastern walls, allowing the latter part of the volcano's evolution to be studied. The lower part of this succession is dominated by andesites, 0.33–0.55 my old (Fig. 9), whereas the upper part is dominated by rhyolite and basalt, 37–51 thousand years old (Fig. 10). We did not observe an obvious erosional unconformity or soil horizon in any of the sections. The identification of rounded cobbles at *ca* 700 m depth during dive R785 (Fig. 10c) supports the inference that WRV was a small island at times. These cobbles might have formed by wave action on a WRV beach before caldera collapse and thermal subsidence of the extinct volcano.

West Rota's large caldera formed in association with a major eruption of felsic magma. Assuming the volcano originally rose to 300 m above sealevel, a conservative estimate based on linear extrapolation of the slopes, the volcano lost approximately 40 km^3 during caldera collapse. If this is equivalent to the volume of magma erupted in a single

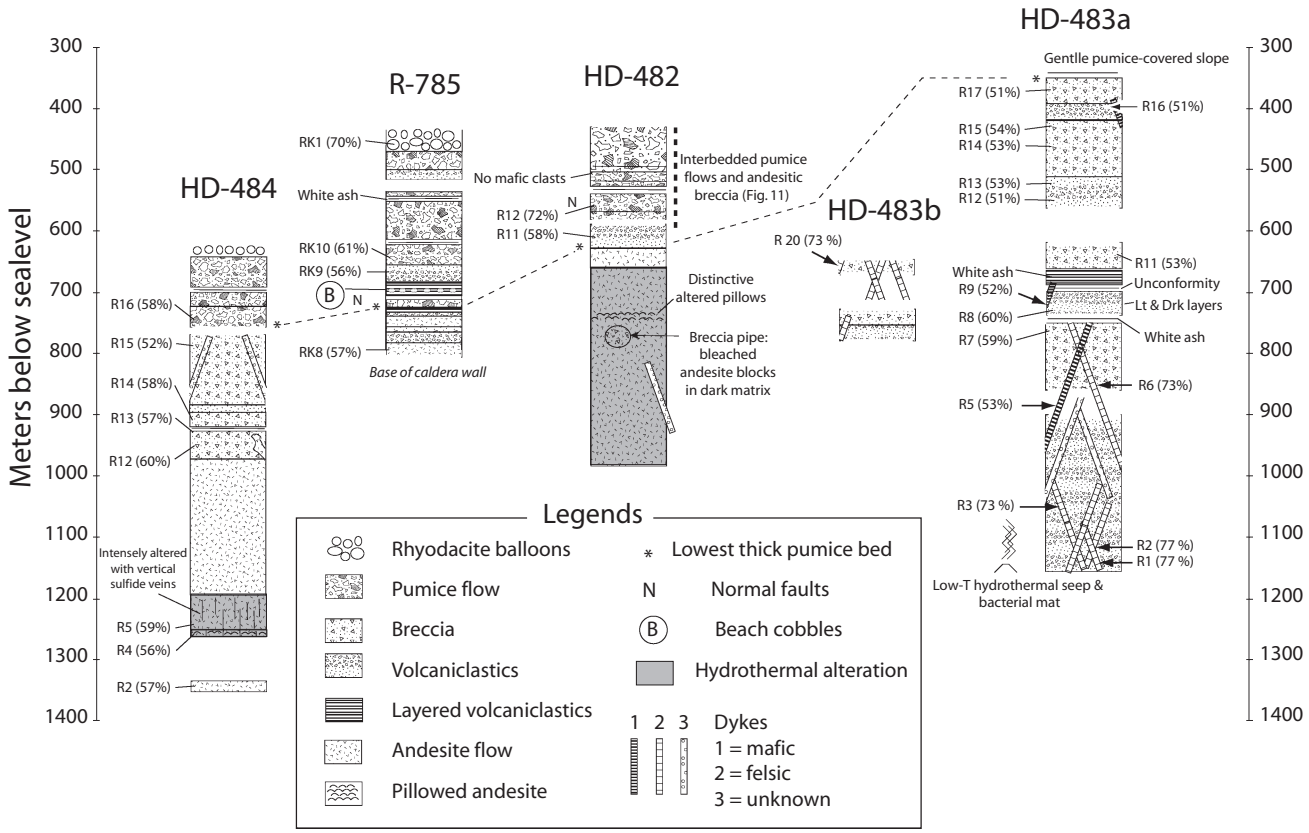

Fig. 8 Summary of stratigraphic sections observed during four remotely operated vehicle (ROV) transects in caldera wall. Note HD-483 is broken into two segments, HD-483 A and HD-483B. Positions of rock samples (numbers with 'R') are given, and in some cases analyzed silica contents. Dashed line shows the detailed section shown in Figure 11.

episode, it implies a very explosive eruption, with Volcanic Explosivity Index *ca* 6 + (Newhall & Self 1982). The WRV Caldera floor shows no evidence of postcollapse magmatic activity in the form of resurgent domes or cones. Tow-Yo surveys with a CTD (conductivity, temperature, depth) instrument package found a weak hydrothermal plume within the caldera (Embley *et al.* 2003), and a small area of low temperature diffuse venting was discovered on dive HD-483a near the base of the southeastern caldera wall (Figs 7,9b). The lack of an active high-temperature hydrothermal system and the geochronological results reported above indicate that WRV is an extinct or long-dormant volcano.

LOWER ANDESITE AND HYDROTHERMAL ALTERATION

The lower part of the volcanic section exposed in the caldera walls comprises fresh and altered andesites along the three northern dives and bimodal dyke swarms in the southeast dive (Fig. 7). Exposures of hydrothermally altered andesite were observed during dives HD-484 (>1200 m BSL) and HD-482 (>750 m BSL). The basal andesitic section was affected by intense hydrothermal alteration and sulphide stockwork mineralization, which – because the overlying basalt-rhyolite section is not altered or mineralized – seems to pre-date caldera collapse. This was the root zone of a robust hydrothermal system, the sea floor expression of which has not been found (and might not exist if hydrothermal activity occurred while WRV was an island). After Cook 7 dredging, we suspected that hydrothermally altered rocks were exposed in the eastern caldera wall because these were abundant in Cook 7 Dredge 63. We did not find these exposures during the single TT-167 dive but encountered them during the Hyper-Dolphin dives. Studies of these dredge samples indicate that alteration was caused by intense flow of high-temperature water, which circulated between the sea floor and a shallow magma reservoir. Fluid circulation reflects very high ratios of water to rock that removed Na_2O and introduced K_2O into the affected rocks (Fig. 5a,

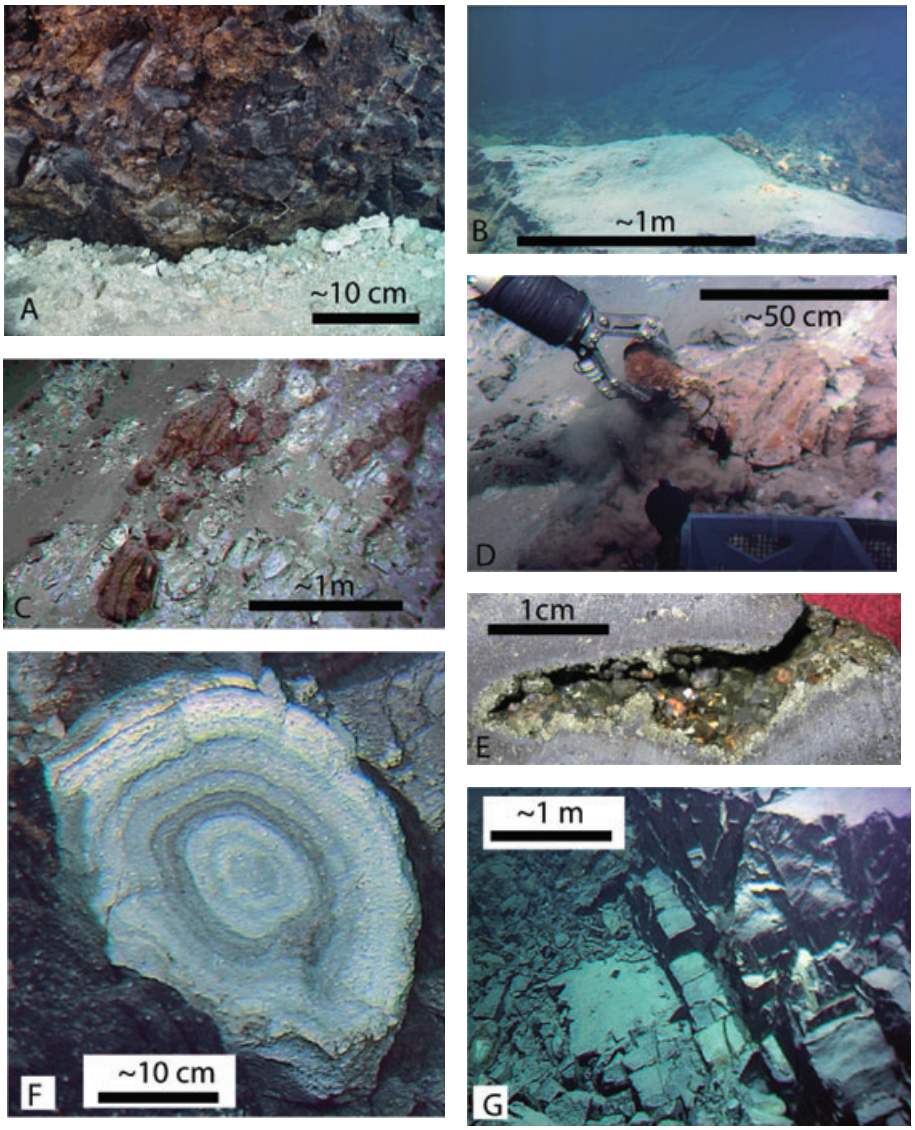

Fig. 9 Photographs taken of lower section observed in eastern caldera wall exposures. (a) Base of vertical caldera wall, white pumice in caldera floor against dark andesites at base of wall (R785, 800 m water depth). (b) Gray mound of fine sediments associated with weak hydrothermal vent at southeast base of caldera wall. Note hydrothermal crusts above the mound to the right (HD-483, 1150 m water depth). (c) Outcrops of hydrothermally altered andesites (bleached white) and resistant ribs of sulphide mineralization (red-brown; HD-484, 1260 m water depth). (d) Sampling 484R6 from sulphide mineralized rib, same location as c. (e) Photograph of cut slab of HD-484R6 taken at d. Note pyrite and chalcopyrite lining vug. (f) Spheroidally altered pillowed andesite (HD-482, 759 m water depth). (g) Dacitic dykes near base of southeast caldera wall (HD-483, 1050 m water depth).

right panel), similar to 'porphyry copper-type' alteration observed at Manzi Seamount farther north in the IBM Arc (Ishizuka *et al.* 2002). Altered samples from Dredge 63 also have disseminated sulphide mineralization. Hydrothermally altered exposures observed during dives HD-484 and HD-482 appear as pervasive bleaching of volcanic rocks. The clay-rich parts are weak, but silicified portions are resistant and stand out as a network of irregular, cross-cutting veins (Fig. 9c). A distinctive horizon observed during dive HD-482 at *ca* 750 m BSL consists of rocks with concentric alteration zones, which appear to preserve original pillow structures (Fig. 9f). These hydrothermally altered pillow basalts are similar to those observed on the Galapagos Ridge (Embley *et al.* 1988). Exposures of hydrothermally altered rocks examined during dive HD-484 include resistant, rust-brown colored ribs that are rich in sulphides (Fig. 9c–e).

CALDERA-FORMING ERUPTION(S)

The upper *ca* 150 m traversed during dive HD-482 is subdivided into four units distinguished on the basis of orange-colored alteration zones on underlying units (Fig. 11). These alteration zones might reflect baking of the underlying material by the overlying pyroclastic flow. Alternatively, the alteration could be iron oxidation of a former sea floor surface or enhanced microbial iron oxidation induced by hydrothermal cooling of the lower flow. In any case, these alteration zones appear to mark surfaces that have been exposed on the sea floor for some time and thus provide a way to subdivide the stratigraphy into four units.

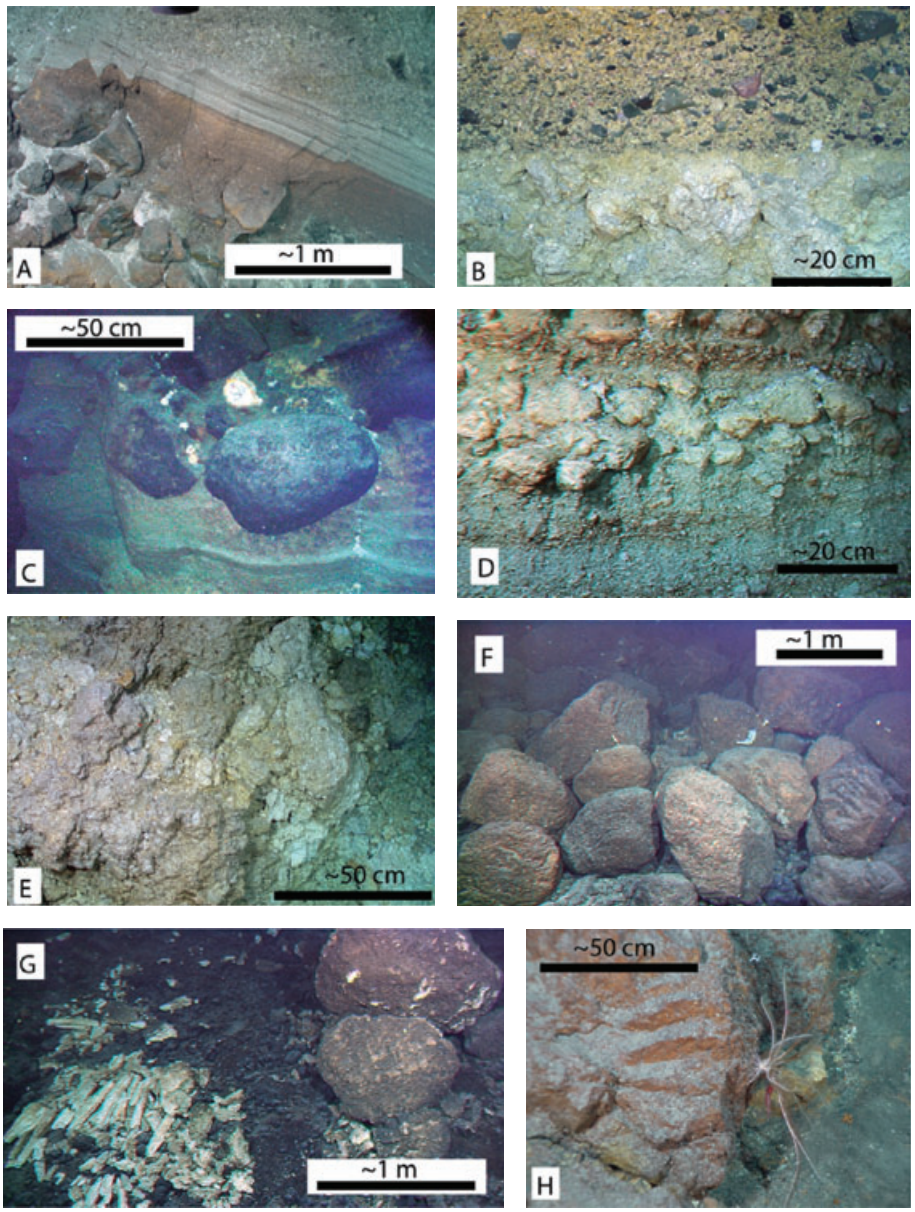

Fig. 10 Photographs of upper section observed in eastern caldera wall, summit rim and southeast parasitic cones. (a) Rhyolitic volcaniclastics overlying basaltic volcaniclastics, R785 724 mbsl. (b) Palagonite-rich basaltic volcaniclastic overlying coarse rhyolite pumice flow, R785 544 m below sealevel (BSL). (c) Possible beach cobble embedded with other cobbles in volcaniclastic layered sands, R785 700 m BSL. (d) Upward-coarsening layered rhyolitic volcaniclastics, thick orange horizon near top of photo subdivide the stratigraphy, HD-482, 555 m BSL. (e) Coarse pumice flow, R785 472 m BSL. (f) Large pieces of rhyolite pumice 'balloons', HD-489, 667 m BSL. (g) Two rhyolite balloons (right) and exploded columns from a broken balloon (left) HD-489, 749 m BSL. (h) Section of balloon showing radial columnar structure and crinoid, R785.

The uppermost unit, Unit D, is an excellent example. This *ca* 75 m thick unit shows overall inverse grading and coarse intervals contain little ash. Rhyolite pumice clasts are angular and as large as *ca* 0.5 m near the top of the unit. Faint bedding was observed near the base. Bedding is sometimes expressed by *ca* 1 m thick layers of pumice sandwiched between thinner (<10 cm) horizons dominated by mafic clasts. Underlying units B and C are well-bedded but also show well-developed reverse grading, with fine pumice showing well-defined bedding at the base grading upwards into increasingly coarse and massive pumice at the top.

Upward coarsening of pumice clasts in each layer (Fig. 10d) is typically produced by subaqueous pyroclastic eruptions (Kano *et al*. 1996). Multiple units can be produced by intermittent eruption-column collapses. This stratigraphy suggests that violent eruptions accompanying caldera formation did not occur as a single episode, as also reflected by the lowermost thick felsic bed observed during dive R785, *ca* 765 m BSL, which is pervasively affected by numerous penecontemporaneous normal faults (Fig. 10a). There might have been a long period of development of one caldera or perhaps formation of multiple calderas.

All four units in Figure 11 are Type 1 subaqueous pumice deposits according to the classification of Kano (2003). Type 1 deposits are thought to form by submarine plinian or flow-generating

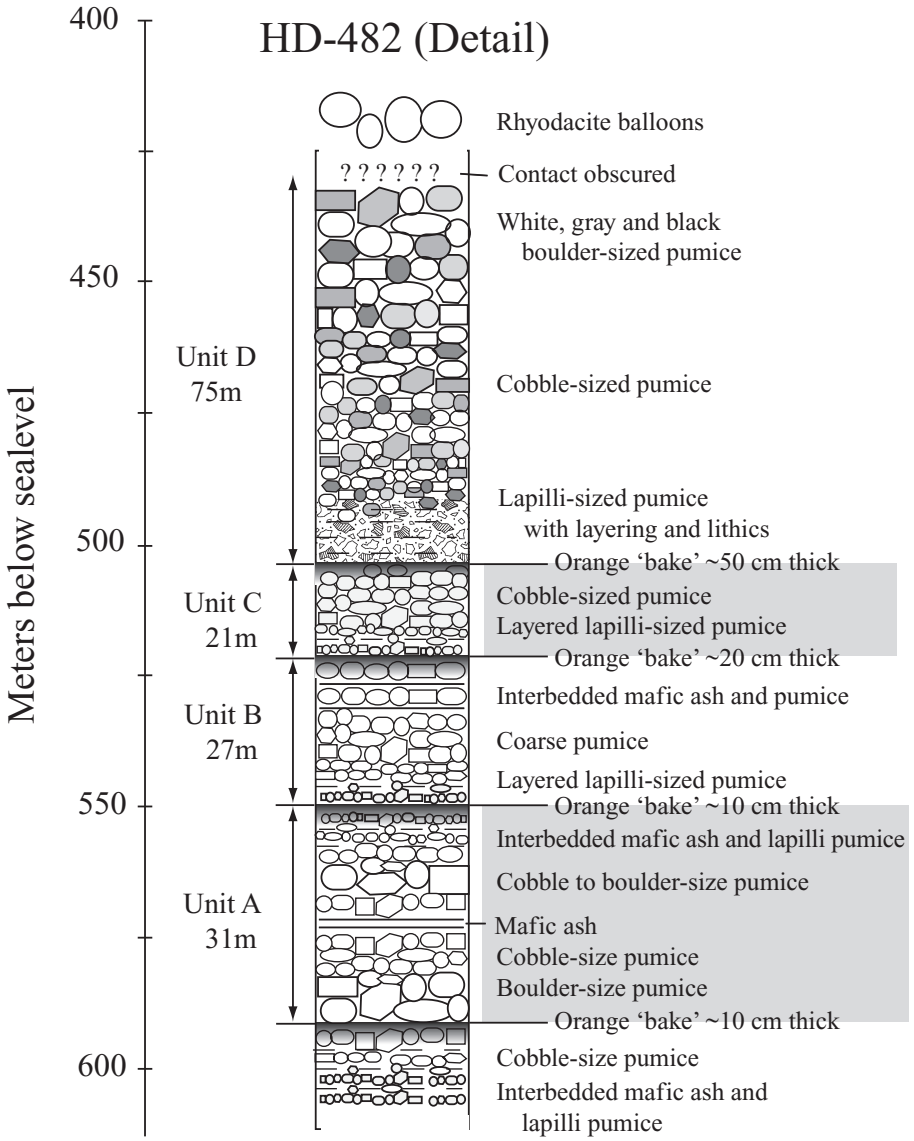

Fig. 11 Detail of upper pyroclastic succession observed during HD-482, stratigraphic position shown by dashed line in Figure 8. Four units are identified, separated by what might be bake zones (see text for further discussion). Note the general reverse grading of units, particularly unit D.

eruptions at water pressures low enough to allow violent vesiculation, corresponding to depths from a few hundred meters down to one thousand meters depending on the magma water content. Because Unit D is very thick (75 m at dive HD-482) and is the youngest Type 1 deposit of WRV, eruption of Unit D was probably associated with formation of the present caldera. Despite its great thickness, it is not welded; welding was not observed in any of the felsic units on WRV, further supporting an interpretation of submarine eruption.

We have not identified the vents responsible for these eruptions. Because the pyroclastic sections seem to thicken northwards (Fig. 8), the vents might lie in the northern part of WRV, perhaps along the WRF. Where the caldera-forming rhyolitic pyroclastic succession is observed (Fig. 11), mafic and felsic components are interbedded everywhere except at the very top of the section (Fig. 10a,b). This suggests that injections of mafic magma stimulated felsic eruptions.

Exposures of the lower caldera wall examined during HD-483 are dominated by nearly vertical mafic and felsic dykes (Fig. 9g). These comprise a northwest–southeast-trending dyke swarm, which might be related to several small basaltic parasitic cones on the southeast flank of WRV (Figs 3,7). The similarity of northwest–southeast directional trend, stratigraphic position and composition of the basalts indicates that the southeast caldera wall dykes and south–east-trending chain of basaltic parasitic cones (HD-489 followed northwest–southeast-trending basaltic dykes *ca* 1150 m BSL)

marks an important locus of late magmatic activity for WRV. A culminating progression from felsic to mafic magmatism with time could be also reflected in the fact that all three mafic (51–53 wt% SiO_2) dykes were sampled <900 m deep, whereas the felsic (73–77 wt% SiO_2) dykes are all from >850 m deep (Fig. 8). The southeast base of caldera wall is also where a low-temperature hydrothermal seep was found (Fig. 9b). This southeast sector of WRV does not seem to be the locus of voluminous rhyolite eruptions associated with caldera formation, because the volcanic sequence as shallow as 350 m is dominated by mafic volcaniclastics and breccias (Fig. 8).

The parasitic cones on the upper southeast slope of the volcano, which were sampled by Cook 7 D64 and 65 and NT05-17 HD-489 (Figs 3,7), are also dominantly basaltic (*ca* 51 wt% SiO_2), with subordinate felsic material. The parasitic cones on the southeast flank of WRV are only covered by large rhyolite pumice 'balloons', the youngest, post-caldera and quiet WRV eruptive products, as discussed below. Basaltic volcanism is not recognized on the caldera floor; this combined with the *ca* 0.47 Ma age for a dacite (HD-489R19) recovered from one of the southeast cones indicates that the northwest–southeast volcanic zone was active before the caldera collapse. The absence of thick pumice pyroclastic deposits (Units A–D, discussed above) in the southeast volcanic zone further suggests that WRV caldera-forming pyroclastic eruptions were directed westward.

RHYOLITE PUMICE 'BALLOONS'

Above the coarse pumice flows, 1–2 m diameter rhyolite balloon-like pumices define the top of the volcanic section (Fig. 10f–h). In contrast to the underlying thick rhyolitic units, the balloons were not erupted violently and thus are thought to reflect relatively quiet eruption of gas-rich rhyolite magma at the final stage of caldera collapse. The pumice balloons have very low density, as shown by the fact that they move significantly when the ROV gently bumped into them, reflecting their vesicular, pumiceous nature. The pumice balloons erupted and cooled in this shape because they often have interior cooling structures – radial columns – that indicate the rounded exterior of the balloons was established while the inside of the balloon was still partially molten (Fig. 10g,h; schematically represented in Fig. 12). These pumice spheres were clearly erupted differently than the older felsic pyroclastics, which

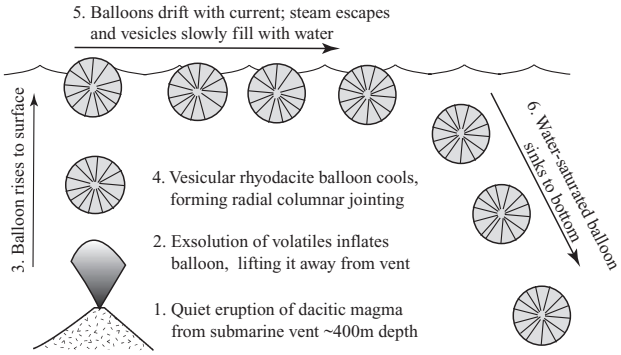

Fig. 12 Summary diagram for the formation of giant rhyolite balloons shown in Figure 10f–h.

are obviously fragmental, broken into angular blocks during eruption and subaqueous transport; these fragments are also much smaller than the 'balloons'.

The large pumices might have formed as a result of quiet extrusion of vesicular rhyolite magma (70 wt% SiO_2) into water (e.g. Allen & McPhie 2000). Explosive fragmentation of such partially degassed hydrous felsic magmas might have been arrested because of hydrostatic pressure at several hundred meters water depth. They are similar in size and internal structure to the 'Giant pumice' of Sierra la Primavera, Mexico (Clough *et al.* 1981). Similar giant pumices were observed to rise to the surface during the 1934–1935 eruption at Kikai Caldera and then slowly sink again (Matumoto 1943). Observations made using Shinkai 2000 manned submersible found pumice blocks that were probably from this eruption, some 12 m long, resting unbroken on the Kikai Caldera floor (Nakamura *et al.* 1986). Hydrostatic pressure must have been great enough that exsolution of water vapor within the extruded magma was not violent, allowing steady inflation of a coherent rhyolitic magma to the point that its bulk density decreased sufficiently to rise into the water column, but could not be so great that vesiculation was impeded. Fiske *et al.* (2001) suggested an optimal depth of *ca* 300 m BSL, corresponding to a pressure of *ca* 30 atmospheres, for the formation of giant rhyolite 'floaters' in the caldera-forming eruption of the Myojin-knoll caldera of the Izu Arc. After the balloons detached from the submarine vent, they floated to the surface, cooling sufficiently slowly to produce radial columnar jointing (Fig. 10g,h). Whitham and Sparks (1986) and Kano *et al.* (1996) infer that the buoyancy of large pumice floaters was short-lived, however, as rapid cooling and condensation of steam created partial

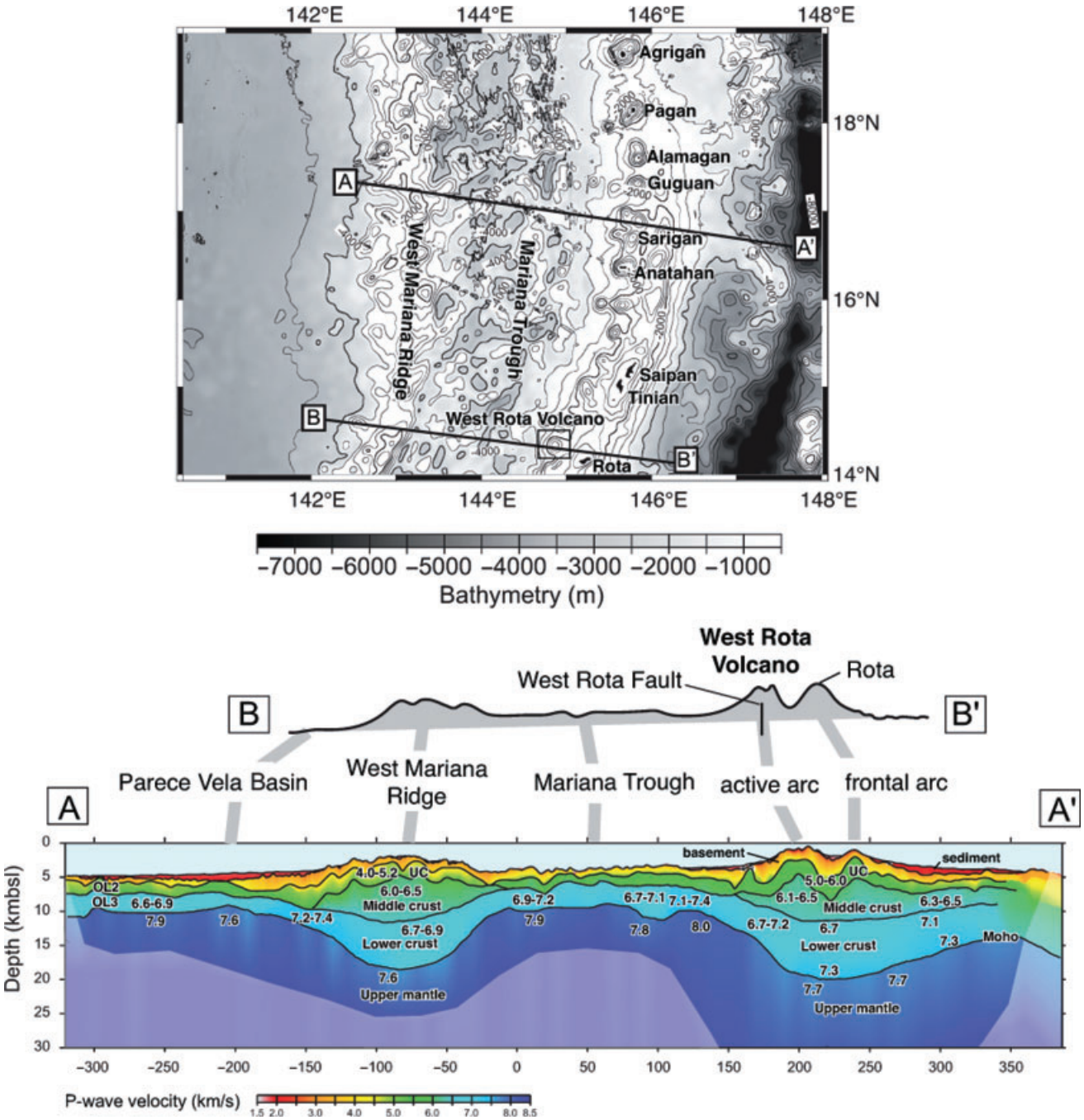

Fig. 13 Simplifed crustal structure of the Mariana Arc near 17°N along section A-A′ after Takahashi *et al.* (2007). Upper crust (UC): mostly mafic lavas and dykes; middle crust: Tonalite, felsic plutons; lower crust: Gabbroic material (Kodaira *et al.* 2007). A mid-crustal felsic layer was inferred for the Mariana Arc near 17°N by Takahashi *et al.* (2007). We can expect similar structure beneath West Rota. Bathymetric profile B-B′ (Takahashi pers. comm., 2007) shows the location of the West Rota Volcano and West Rota Fault relative to the mid-crustal felsic layer. The fault might tap the felsic layer when mafic magma is injected into the mid-crustal layer.

vacuums in vesicles, drawing in seawater, gradually increasing floater bulk density until they sank. Our idea for how the rhyolite balloons formed and were distributed around the volcano, is based on figure 13 of Allen and McPhie (2000) and is summarized in Figure 12.

DO WEST ROTA VOLCANO FELSIC MAGMAS COME FROM THE MID-CRUSTAL FELSIC LAYER?

The origin of felsic magmas in juvenile, intraoceanic arcs is of great interest to the broad geological community. Basu (2006) and Shukuno *et al.*

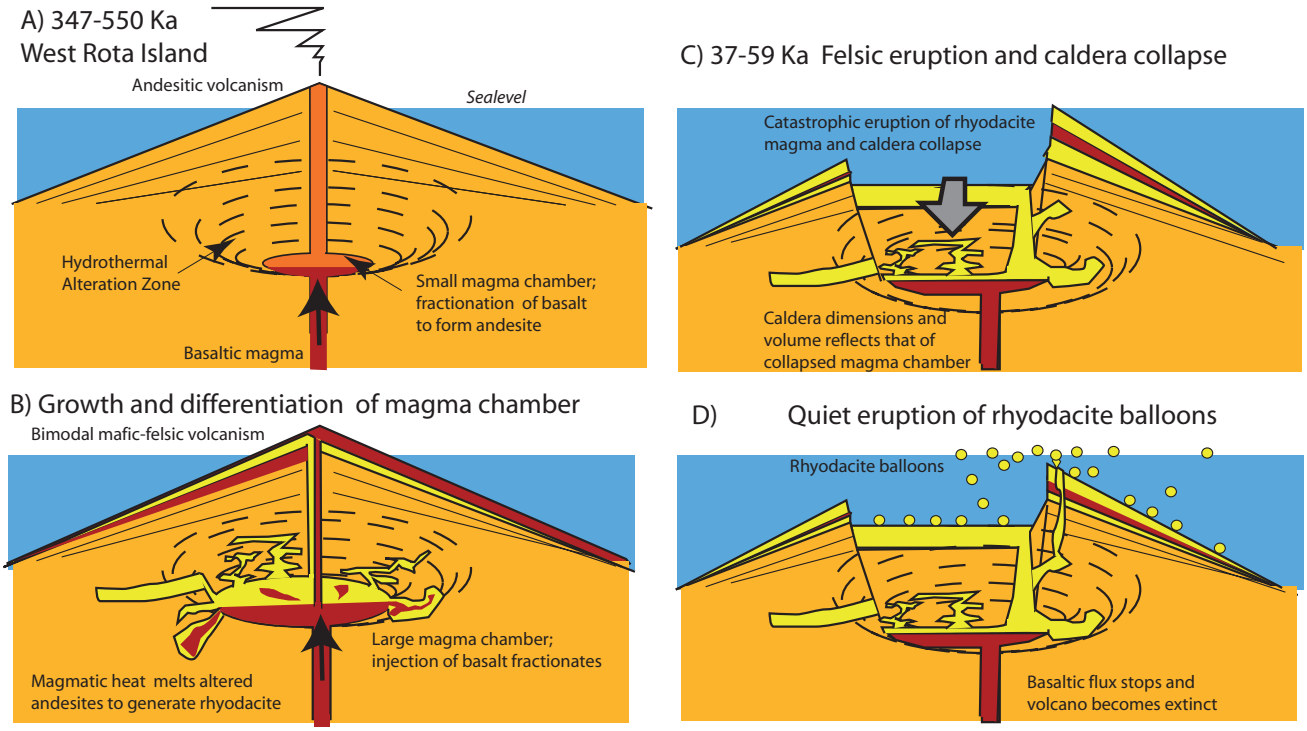

Fig. 14 Schematic evolution of West Rota volcano, Late Pleistocene time. (a) Development of andesitic stratovolcano, probably forming small island. Volcano had a magma reservoir where andesite formed by fractionation of basalt, either directly beneath the volcano or in the middle crust. Hydrothermal system developed during this time. (b) Basaltic magma flux melts altered andesites to form rhyolite and larger magma reservoir system. (c) A series of catastrophic eruptions of rhyolite magma caused collapse of magma reservoir system and formation of caldera. (d) The final stage of caldera-forming magmatism produces parasitic basaltic cones on southeast slope of volcano. Large pumices form during last stages of felsic magmatism finishing caldera formation.

(2006) concluded that WRV felsic magma was generated by anatexis of andesitic material under amphibolite-facies pressure–temperature (*P–T*) conditions corresponding, as a result of heat supplied by injection of basaltic magma. A similar interpretation is generally accepted for the formation of felsic magmas in the Izu Arc (Kawate & Arima 1998; Tamura & Tatsumi 2002; Shukuno *et al.* 2006) and the Kermadec Arc (Smith *et al.* 2003a,b). A mid-crustal felsic layer was inferred for the Mariana Arc near 17°N by Takahashi *et al.* (2007). Middle crust with the seismic velocity measured and shown of Figure 13 will be composed of silicic plutons containing more than 64 wt% high SiO_2 (Kitamura *et al.* 2003; Kodaira *et al.* 2007). This could be the ultimate source of WRV felsic material.

The occurrence of a voluminous felsic eruption, not found elsewhere in the Mariana Arc, might reflect the fact that WRV is located on a major normal fault (WRF), which allows magmas stored in the mid-crustal felsic melt to easily move to the surface. Figure 13 interprets and modifies the seismic crustal structure of Takahashi *et al.* (2007) to show the location of the WRV and WRF relative to the mid-crustal felsic layer, and how the fault might tap the felsic layer when mafic magma is injected into it.

VOLCANIC HISTORY AND CONCLUSIONS

Our understanding of the volcanic history of WRV is fragmentary and incomplete. Nevertheless, the broad outlines of its evolution are clear, as shown in Figure 14. Uplift of the southern Mariana forearc associated with rapid rollback along the Challenger Deep segment of the Mariana Trench resulted in large offsets along the WRF. Mantle-derived magma exploited this weakness, forming a volcano near the fault's northern terminus. Andesitic volcanism led to formation of a large submarine volcano before *ca* 0.5 Ma, with growth of a magma chamber where fractionation of basalt or magnesian andesite to form andesite occurred. The growing volcano eventually rose above sea-level to form an island. A vigorous hydrothermal system associated with sulphide mineralization

developed, pervasively altering parts of the andesitic succession. Anatexis of amphibolite-facies andesitic rocks formed felsic melts, perhaps at mid-crustal depths. A series of violent submarine felsic pyroclastic eruptions accompanied formation of a large caldera, triggered by a new influx of mafic magma, renewed movements along the WRV fault, or both. Vents for the culminating eruptions have not been identified but might lie in the northern part of the WRV. Igneous activity during and after caldera collapse formed small parasitic cones along a south–east-trending neovolcanic zone. The final activity of WRV was relatively quiet, generating giant rhyolite pumice balloons.

ACKNOWLEDGEMENTS

We are indebted to Captain F. Saito of R.V. *Natsushima* and their crews, Operation Manager K. Chiba and the operation team of the ROV HyperDolphin. We thank Dr N. Takahashi for preparing Figure 13. We thank Dr K. Kano, Dr Bill Chadwick, and two anonymous reviewers for their careful and insightful reviews of two versions of this manuscript. This work was supported by JSPS Grant-in-Aid for Scientific Research (B) (17340165) (YT) and NSF grant 0405651 (RJS). RJS is grateful for travel support from the NOAA Pacific Marine Environmental Laboratory for a research stay at PMEL during July 2006. The NOAA Ocean Exploration Program supported the 2003–2004 programs during which much of the multibeam data was collected and one of the dives (R-785) was made. This is a contribution to the NSF-MARGINS program and is UTD Geosciences contribution #1111 and PMEL contribution number 3090.

REFERENCES

ALLEN S. R. & MCPHIE J. 2000. Water-settling and resedimentation of submarine rhyolitic pumice at Yali, eastern Aegean, Greece. *Journal of Volcanology and Geothermal Research* **95**, 285–307.

BASU N. K. 2006. Geology and geochemistry of West Rota, a large submarine caldera in the Southern Mariana Arc. MS Thesis, University of Texas at Dallas, Richardson, 99 pp.

BLOOMER S. H., STERN R. J. & SMOOT N. C. 1989. Physical volcanology of the submarine Mariana and Volcano Arcs. *Bulletin of Volcanology* **51**, 210–24.

CLOUGH B. J., WRIGHT J. V. & WALKER G. P. L. 1981. An unusual bed of giant pumice in Mexico. *Nature* **289**, 49–50.

DIXON T. H. & STERN R. J. 1983. Petrology, chemistry, and isotopic composition of submarine volcanoes in the southern Mariana arc. *Geological Society of America, Bulletin* **94**, 1159–72.

EDWARDS M. 2007. HIGP acoustic wide-angle imaging instrument [online]. Available from: http://www.soest.hawaii.edu/HMRG/MR1/.

EMBLEY R. W., CHADWICK W. W., BAKER E. T., JOHNSON P. D., MERLE S. G. & RISTAU S. 2003. New mapping of Mariana submarine volcanoes with side-scan and multibeam sonars. *Eos Transaction American Geophysical Union* **84**, Abstract T32A-0913.

EMBLEY R. W., CHADWICK W. W., BAKER E. T. *et al.* 2006. Long-term eruptive activity at a submarine arc volcano. *Nature* **441**, 494–7.

EMBLEY R. W., JONASSON I. R., PERFIT M. R. *et al.* 1988. Submersible investigation of an extinct hydrothermal system on the Galapagos Ridge: Sulfide mounds, stockwork zone, and differentiated lavas. *Canadian Mineralogist* **26**, 517–40.

FISKE R. S., NAKA J., IIZASA K., YUASA M. & KLAUS A. 2001. Submarine silicic caldera at the front of the Izu-Bonin Arc, Japan: Voluminous seafloor eruptions of rhyolite pumice. *Geological Society of America Bulletin* **113**, 813–24.

FLECK R. J., SUTTER J. F. & ELLIOT D. H. 1977. Interpretation of discordant $^{40}Ar/^{39}Ar$ age-spectra of Mesozoic tholeiites from Antarctica. *Geochimica. Cosmochimica Acta* **41**, 15–32.

FRYER P., BECKER N., APPELGATE B., MARTINEZ F., EDWARDS M. & FRYER G. 2003. Why is the Challenger Deep so deep? *Earth and Planetary Science Letters* **211**, 259–69.

GILL J. B. 1981. *Orogenic Andesites and Plate Tectonics*. Springer-Verlag, New York.

GVIRTZMAN Z. & STERN R. J. 2004. Bathymetry of Mariana trench-arc system and formation of the Challenger Deep as a consequence of weak plate coupling. *Tectonics* **23**, doi:10.1029/2003TC001581.

ISHIHARA T., STERN R. J., FRYER P., BLOOMER S. & BECKER N. C. 2001. Seafloor spreading in the southern Mariana Trough inferred from 3-component magnetometer data. *EOS Transaction American Geophysical Union* **82**, Abstract T41C-0895.

ISHIZUKA O., UTO K. & YUASA M. 2003. Volcanic history of the back-arc region of the Izu-Bonin (Ogasawara) arc. *Geological Society Special Publication* **219**, 187–205.

ISHIZUKA O., YUASA M. & UTO K. 2002. Evidence of porphyry copper-type hydrothermal activity from a submerged remnant back-arc volcano of the Izu-Bonin arc: Implications for the volcano-tectonic history of back-arc seamounts. *Earth and Planetary Science Letters* **198**, 381–99.

KANO K. 2003. Subaqueous pumice eruptions and their products: A review. *In* White J. D. L., Smellie J. L. & Clague D. A. (eds). Explosive Subaqueous Volcanism.

Geophysical Monograph **140**, 213–29. AGU, Washington, DC.

KANO K., YAMAMOTO T. & ONO K. 1996. Subaqueous eruption and emplacement of the Shinjima Pumice, Shinjima (Moeshima) Island, Kagoshima Bay, SW Japan. *Journal of Volcanology and Geothermal Research* **71**, 187–206.

KATO Y. 2007. 3,000 m Class Remotely Operated Vehicle HYPER-DOLPHIN [online]. Available from: http://www.jamstec.go.jp/e/about/equipment/ships/hyperdolphin.html.

KATO T., BEAVAN J., MATSUSHIMA T., KOTAKE Y., CAMACHO J. T. & NAKANO S. 2003. Geodetic evidence of back-arc spreading in the Mariana Trough. *Geophysical Research Letters* **30**, doi:10.1029/2002GL016757.

KAWATE S. & ARIMA M. 1998. Petrogenesis of the Tanzawa plutonic complex, central Japan: Exposed felsic middle crust of the Izu-Bonin-Mariana arc. *Island Arc* **7**, 342–58.

KITAMURA K., ISHIKAWA M. & ARIMA M. 2003. Petrological model of the northern Izu-Bonin-Mariana arc crust: Constraints from high-pressure measurements of elastic wave velocities of the Tanzawa plutonic rocks, central Japan. *Tectonophysics* **371**, 213–21.

KODAIRA S., SATO T., TAKAHASHI N. *et al.* 2007. Seismological evidence for variable growth of crust along the Izu intra-oceanic arc. *Journal of Geophysical Research* **112**, B05104, doi:10.1029/2006JB004593.

KOHUT E. J., STERN R. J., KENT A. J. R., NIELSEN R. L., BLOOMER S. H. & LEYBOURNE M. 2006. Evidence for adiabatic decompression melting in the southern Mariana arc from high-Mg lavas and melt inclusions. *Contributions to Mineralogy and Petrology* **152**, 201–21.

LANPHERE M. A. & BAADSGAARD H. 2001. Precise K-Ar, $^{40}Ar/^{39}Ar$, Rb-Sr and U/Pb mineral ages from the 27.5 Ma Fish Canyon Tuff reference standard. *Chemical Geology* **175**, 653–71.

LIPMAN P. W. 1997. Subsidence of ash-flow calderas: Relation to caldera size and magma-chamber geometry. *Bulletin of Volcanology* **59**, 198–218.

MARTINEZ F., FRYER P. & BECKER N. 2000. Geophysical characteristics of the southern Mariana Trough, 11°50′N-13°40′N. *Journal of Geophysical Research* **105** (16), 591–607.

MATUMOTO T. 1943. The four gigantic caldera volcanoes of Kyusyu. *Japanese Journal of Geology and Geography* **19**, 1–57.

MERLE S. & CAROTHERS K. 2007. Mariana Arc [online]. Available from: http://www.oceanexplorer.noaa.gov/explorations/06fire/background/marianaarc/marianaarc.html.

MILLER M. S., GORBATOV A. & KENNETT B. L. N. 2006. Three-dimensional visualization of a near-vertical slab tear beneath the southern Mariana arc. *Geochemistry Geophysics Geosystems* **7**, doi:10.1029/2005GC001110.

NAKAMURA K., SAKAGUCHI K. & NAGAI T. 1986. Marine geological survey in the Kikai caldera with special reference to the occurrence of giant pumices, the detailed survey on topography and the measurement of sea water temperature. *Technical Report of the Japan Marine Science and Technology Center, Second Symposium in Deep Sea Research Using the Submersible Shinkai 2000 System*, pp. 137–55 (in Japanese with English Abstract).

NEWHALL C. G. & SELF S. 1982. The volcanic explosivity index (VEI) – an estimate of explosive magnitude for historical volcanism. *Journal of Geophysical Research* **87**, 1231–8.

ROGNSTAD M. 1992. Hawaii MR1: A new underwater mapping tool. *International Conference on Signal Processing and Technology*, November 1992, Honolulu, USA, pp. 900–5.

SHEPHERD K. 2007. Ropos.com: Canadian Scientific Submersible Facility [online]. Available from: http://www.ropos.com/.

SHUKUNO H., TAMURA Y., TANI K., CHANG Q., SUZUKI T. & FISKE R. S. 2006. Origin of silicic magmas and the compositional gap at Sumisu submarine caldera, Izu-Bonin arc, Japan. *Journal of Volcanology and Geothermal Research* **156**, 187–216.

SMITH W. H. F. & SANDWELL D. 1997. Global sea floor topography from satellite altimetry and ship depth soundings. *Science* **277** (5334), 1956–62.

SMITH I. E. M., STEWART R. B. & PRICE R. C. 2003a. The petrology of a large intra-oceanic silicic eruption. The Sandy Bay Tephra, Kermadec Arc, Southwest Pacific. *Journal of Volcanology and Geothermal Research* **124**, 173–94.

SMITH I. E. M., WORTHINGTON T. J., STEWART R. B., PRICE R. C. & GAMBLE J. A. 2003b. Felsic Volcanism in the Kermadec Arc, SW Pacific: Crustal recycling in an oceanic setting. *In* Larter R. D. & Leat P. T. (eds). Intra-oceanic Subduction Systems: Tectonic and Magmatic Processes. *Geological Society of London Special Publication*, pp. 99–118.

STERN R. J., FOUCH M. J. & KLEMPERER S. 2003. An overview of the Izu-Bonin-Mariana subduction factory. *In* Eiler J. (ed.). *Inside the Subduction Factory, Geophysical Monograph*, Vol. 138, pp. 175–222. AGU, Washington, DC.

TAKAHASHI N., KODAIRA S., KLEMPERER S., TATSUMI Y., KANEDA Y. & SUYEHIRO K. 2007. Crustal structure and evolution of the Mariana intra-oceanic island arc. *Geology* **35**, 203–47.

TAMURA Y. & TATSUMI Y. 2002. Remelting of an andesitic crust as a possible origin for rhyolitic magma in oceanic arcs: An example from the Izu-Bonin Arc. *Journal of Petrology* **43**, 1029–47.

TATSUMI Y. & STERN R. J. 2006. Manufacturing continental crust in the subduction factory. *Oceanography* **19**, 104–12.

UTO K., ISHIZUKA O., MATSUMOTO A., KAMIOKA H. & TOGASHI K. 1997. Laser-heating $^{40}Ar/^{39}Ar$ dating

system of the Geological Survey of Japan: System outline and preliminary results. *Bulletin of Geological Survey of Japan* **48**, 23–46.

WHITHAM A. G. & SPARKS R. S. J. 1986. Pumice. *Bulletin of Volcanology* **48**, 209–23.

WRIGHT I. C., WORTHINGTON T. J. & GAMBLE J. A. 2006. New multibeam mapping and geochemistry of the 30°–35° S sector, and overview of southern Kermadec arc volcanism. *Journal of Volcanology and Geothermal Research* **149**, 263–96.

APPENDIX 1: DATA SYSTEMS MAP

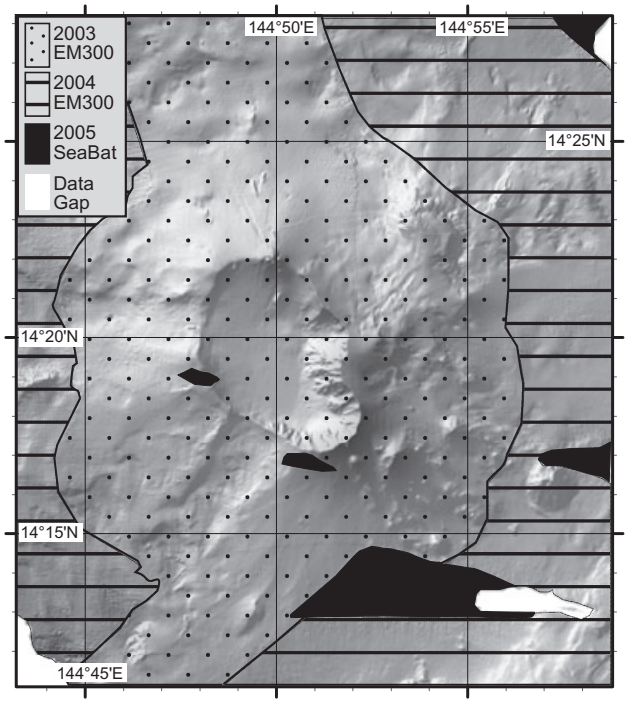

Fig. A1 Same map area as Figure 4 showing the compilation of multibeam bathymetry data sources. EM300 data collected in 2003 and 2004 aboard the R/V *Thomas G. Thompson* were gridded together and stacked on top of SeaBat data collected in 2005 aboard the R/V *Natsushima*. Data grid cell size is 25 m.